Journal of
Composites Science

MDPI

Article

Flame-Retardant and Tensile Properties of Polyamide 12 Processed by Selective Laser Sintering

Tatjana Glaskova-Kuzmina [1,2,*], Didzis Dejus [1], Jānis Jātnieks [1], Partel-Peeter Kruuv [1], Linda Lancere [1], Stepans Kobenko [1], Anatolijs Sarakovskis [3] and Aleksejs Zolotarjovs [3]

[1] Baltic3D.eu, Braslas 22D, LV-1035 Riga, Latvia; didzis@baltic3d.eu (D.D.); janis@baltic3d.eu (J.J.); partel-peeter@baltic3d.eu (P.-P.K.); linda@baltic3d.eu (L.L.); steathl8@gmail.com (S.K.)
[2] Institute for Mechanics of Materials, University of Latvia, Jelgavas 3, LV-1004 Riga, Latvia
[3] Institute of Solid State Physics, Kengaraga 8, LV-1063 Riga, Latvia; anatoly@cfi.lu.lv (A.S.); aleksejs.zol@gmail.com (A.Z.)
* Correspondence: tatjana.glaskova-kuzmina@lu.lv

Abstract: Composite materials are becoming widely applied in fire-critical conditions such as, e.g., aviation interior parts. Environmental considerations motivate the use of additive manufacturing due to the decrease of polymer wastes, and therefore additional fuel sources. The aim of this work was to evaluate the effect of printing direction on flame retardancy and the tensile properties of 3D-printed test samples of polyamide 12 manufactured by selective laser sintering. The effects of printing parameters on the flammability of 3D-printed samples were investigated using vertical burn tests with varied specimen thicknesses and printing directions. It was found that these effects were substantial for the flammability at a low thickness of the test samples. No significant effects of printing direction were revealed for the tensile characteristics of polyamide 12.

Keywords: flame-retardant properties; vertical burn test; tensile properties; anisotropy; additive manufacturing; polyamide 12; selective laser sintering

Citation: Glaskova-Kuzmina, T.; Dejus, D.; Jātnieks, J.; Kruuv, P.-P.; Lancere, L.; Kobenko, S.; Sarakovskis, A.; Zolotarjovs, A. Flame-Retardant and Tensile Properties of Polyamide 12 Processed by Selective Laser Sintering. *J. Compos. Sci.* **2022**, *6*, 185. https://doi.org/10.3390/jcs6070185

Academic Editors: Yingtao Liu and Yirong Lin

Received: 3 June 2022
Accepted: 22 June 2022
Published: 23 June 2022

1. Introduction

Additive manufacturing (AM) is becoming widely applied as a manufacturing process in both aerospace and automotive fields, mainly due to design flexibility, reduction in the design-to-manufacturing cycle time, capability to produce complex shapes without manufacturing restraints, reduction of joints and connections, and a decrease in raw material waste [1–4]. There are also disadvantages to the use of AM, such as, e.g., a small range of available raw materials, restricted build size, postprocessing of the printed parts (cleaning and sanding, water jetting, a chemical soak and wash, air or heat drying, etc.), possible design inaccuracies, and the potential to disrupt the industry and affect employment rates in the long term [3,5]. Nevertheless, AM is a very competitive technology compared to traditional manufacturing approaches such as compression and injection moulding, extrusion, etc., especially for the low-volume fabrication of small parts (e.g., aircraft interior spare parts). Recent numerical and experimental results on the structural integrity of aircraft interior spare parts, a class divider and seat folding table, produced by fused deposition modelling revealed a potential to replace traditionally applied metals [4]. Holding the critical loads that are characteristic of the aircraft interior parts, the 3D-printed parts allowed savings of up to 30% of their weight, which can contribute to the reduction of the total aircraft weight, and can further decrease fuel consumption and CO_2 release.

As a matter of fact, for all materials used in aircraft interior parts, it is crucial to pass the requirements for flammability formulated in FAR 25.853 and FAR 25.855 [6,7]. The aviation industry is one of the most regulated industries because any airborne incident could easily have disastrous results without stringent regulations surrounding materials and their

use [8]. The results for the flame-retardant properties of Ultem 9085 polymer composites processed by fused deposition modelling (FDM) have been reported [9]. The effects of several processing parameters, such as percentage of infill, number of solid layers, and thickness of the samples on the burn length and heat release rate, were revealed to prove that all tested samples could pass the requirements formulated in FAR 25.853 and FAR 25.855.

In general, the flammability performance could be referred to as the reaction-to-fire processes of a substance, which consists of ignitability, flame spread, heat release, and combustion products (e.g., smoke production) [10]. Combustion is defined as a catalytic exothermic reaction maintained by internally generated heat and free radicals [11].

During the exposition to abundant heat, both natural and synthetic polymers, as well as polymer-based composites, will thermally degrade. This process is also known as pyrolysis, which evolves flammable volatiles. Mixed with air at appropriate temperatures, such volatiles will ignite. Ignition can occur either spontaneously (autoignition) or due to the presence of an external source such as a spark or a flame (flash ignition).

SLS is classified as a powder bed fusion method of building objects by sintering powder particles using laser energy [12]. Compared with FDM, due to the high resolution of the laser beam, the SLS technique allows the prodution of 3D parts with a minimal content of voids, which could be neglected [12,13]. The results on flame retardancy for polyamide 12/flame retardant compositions produced by SLS were recently reported [14,15]. It has been shown that some compositions could not be processed because of the insufficient flowing behaviour of blended powders and the ability to keep the necessary temperature range for processing [14]. Moreover, the addition of filler in laser sintering led to changes in the process behaviour and physical properties (optical, thermal, and mechanical) of the component [15]. The printing quality of 3D-printed parts can be evaluated through the mechanical properties by changing production parameters (e.g., raster angle and orientation, layer thickness, raster-to-raster gap etc.) [16–18]. The effect of different reinforcements on the mechanical properties of SLS polyamide 12 has also been discussed [19,20]. Nevertheless, in all these studies, the effect of printing direction for SLS technology and subsequent possible anisotropy of the physical properties (e.g., flame-retardant and mechanical properties) of 3D-printed parts were not analysed.

Therefore, the aim of this work was to evaluate the effect of printing direction on the flame-retardant and tensile properties of polyamide 12 manufactured by SLS by performing vertical burn and quasi-static tensile tests. No similar results were found in the literature.

2. Materials and Methods

2.1. Materials

PA 2241 FR supplied by EOS GmgH (Krailling, Germany) is a polyamide 12-based material that contains a halogen flame retardant [21]. Thanks to its good reusability, it is very cost-efficient compared to other traditional flame-retardant materials. The additively manufactured parts have comparatively high elastic modulus (1.9 GPa) and tensile strength (46–49 MPa), as well as heat deflection temperature (86 °C), allowing this material to be used in the interior of aircraft, e.g., ventilation ducts and exhaust valves. The study material is in the form of white powder and was stored in a vacuum-sealed protective bag. The material that was used for the sample manufacturing was stored at the same temperature (22 °C) and humidity conditions (50% RH); thus, it has the same physical properties before and during the manufacturing.

2.2. Manufacturing of the Test Samples

An EOS P 396 SLS printer (EOS, Krailling, Germany) and the post-processing machine, shown in Figure 1a,b, were used for the manufacturing of all test samples at Baltic3D.eu factory [22]. SLS is a sintered material coating process that uses a laser as a power source and directs the laser to specific points in space attributed to a 3D object [3].

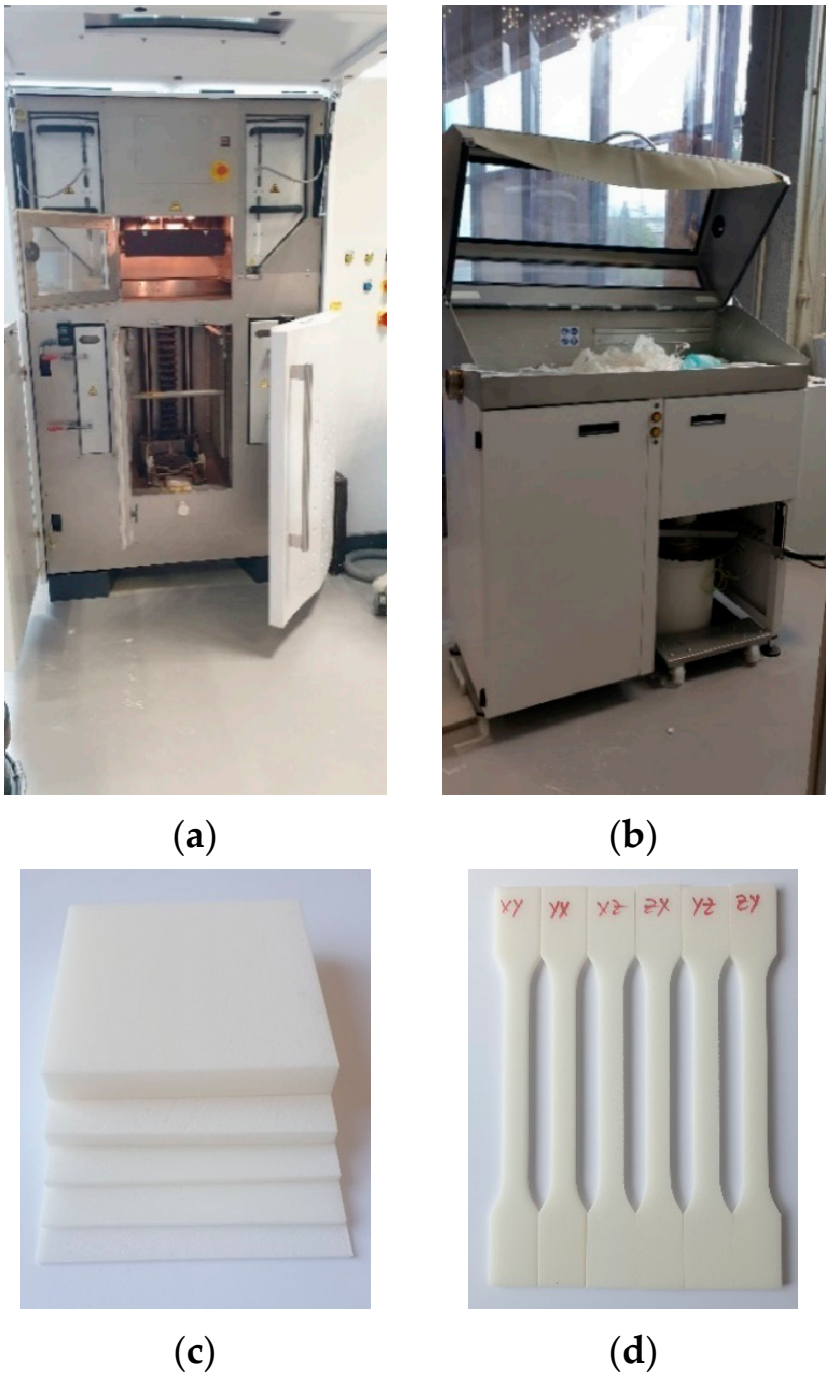

Figure 1. EOS P 396 printer (**a**) and post-processing machine (**b**) at Baltic3D.eu factory; the samples printed in the direction of $XY \pm 45°$ at different thicknesses of 1.00, 1.75, 2.00, 5.00, and 10.00 mm (**c**) and dog-bone samples for tensile tests (**d**).

2.2.1. Test Samples for Vertical Burn Test

For different printing directions, the samples were printed at varying thicknesses (1–10 mm). Some of the samples printed in the direction of $XY \pm 45°$ at different thicknesses are shown in Figure 1c. The printing parameters for the test samples used in vertical burn tests are summarized in Table 1. Full infill density was used for all samples.

Table 1. Printing parameters for the test samples used in vertical burn tests.

Thickness, mm	Printing Direction
1.00	X, Y, Z, $XY \pm 45°$, $ZX \pm 45°$
1.25	X, $XY \pm 45°$, $ZX \pm 45°$
1.50	$XY \pm 45°$, $ZX \pm 45°$
1.75	$XY \pm 45°$, $ZX \pm 45°$
2.00	X, Y, Z, $XY \pm 45°$, $ZX \pm 45°$
2.50	$XY \pm 45°$, $ZX \pm 45°$
3.00	$XY \pm 45°$, $ZX \pm 45°$
4.00	$XY \pm 45°$, $ZX \pm 45°$
5.00	$XY \pm 45°$, $ZX \pm 45°$
6.00	$XY \pm 45°$, $ZX \pm 45°$
7.00	$XY \pm 45°$, $ZX \pm 45°$
8.00	$XY \pm 45°$, $ZX \pm 45°$
10.00	$XY \pm 45°$, $ZX \pm 45°$

After printing, the samples were required to pass post-processing (Figure 1b). It was necessary to accurately remove the excess PA 2241 material that exists in uncured powder form. The dimensions of the samples printed for vertical burn tests were 75 × 305 mm, according to the criteria formulated in FAR 25.853, Appendix F, Part I [6]. Three replicates were printed for each sample configuration.

2.2.2. Test Samples for Tensile Tests

To investigate the effect of printing orientation on tensile properties, the test samples were printed in different planes, such as XY, XZ, and ZY, with a printing orientation set as the second axis. Additionally, the samples were also printed in the YX, ZX, and ZY planes. The rest of the printing parameters were kept constant. The dimensions of the test specimens were 150 × 10 × 4 mm, according to the standard [23]. At least three samples were printed for each design configuration.

2.3. Vertical Burn Tests

The vertical burn tests were performed at Lantal Textiles AG (Langenthal, Switzerland) according to FAR 25.853, Appendix F, Part I of aviation standards. Before the tests, all specimens were conditioned at 22.5 °C and 50% RH until moisture equilibrium was reached. During this test, the resistance of materials to a flame (at a temperature of 843 °C) was tested according to 60-s vertical burn test requirements (V60). Thus, samples with dimensions of 305 mm × 75 mm were suspended vertically (see Figure 2) and a burner was placed 19 mm below the lower leading edge for 60 s, after which the flame was removed. The burner was set to provide a 23 mm core flame and a 38 mm outer flame for all tests. The main parameters of the test are the ignition time, flame time, drip flame time, and burn length. Detailed information about the main parameters has been previously reported by the authors [9]. To pass a 60-s vertical burn test, there are certain requirements for the samples: (1) the average flame time (time until self-extinguishing occurs) shall not exceed 15 s, (2) the average drip extinguishing time shall not exceed 3 s, and (3) the average burn length shall not exceed 152 mm. At least three test samples for each sample configuration (see Table 1) were tested, and the values given correspond to their arithmetic mean value.

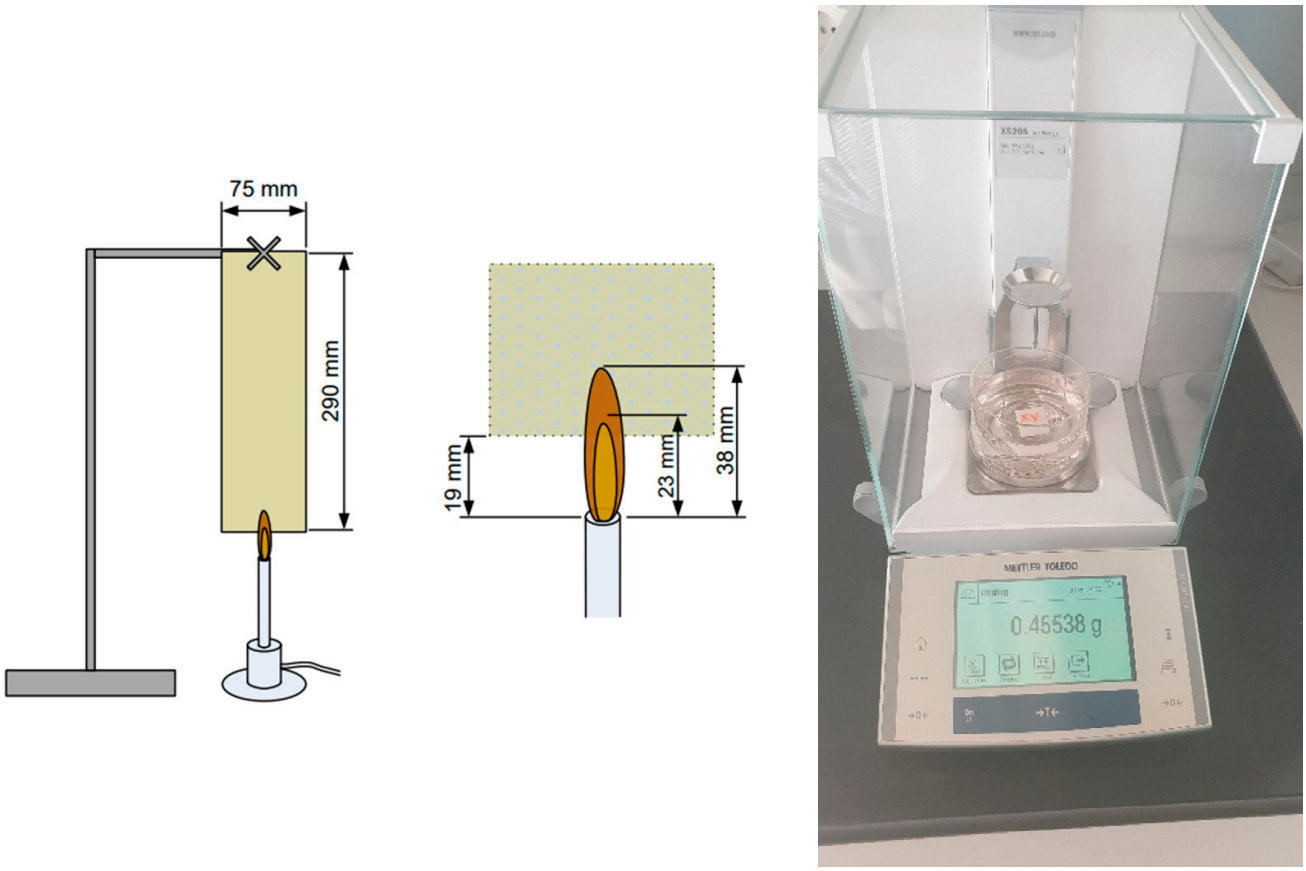

Figure 2. Schematic presentation of a vertical burn test [8] (**a**) and hydrostatic weighting of the test sample printed in *XY* direction (**b**). Reprinted with permission from [8], CC BY-NC-SA 3.0 NZ, 2014, ResearchSpace@Auckland, Maurice Chai.

2.4. Quasistatic Tensile Tests

Quasi-static tensile tests were performed at the University of Latvia for the samples with different printing orientations and printed on different planes (see Figure 3 using a Zwick 2.5 testing machine with a crosshead speed of 2 mm/min at room temperature. Tensile strength was defined as the maximal achieved value of stress in the specimen, and the elastic modulus was calculated from the slope of a secant line between 0.05 and 0.25% strain on a stress–strain plot by using the equation:

$$E = \frac{\sigma_2 - \sigma_1}{\varepsilon_2 - \varepsilon_1}, \quad (1)$$

where ε_1 and ε_2, σ_1 and σ_2 are corresponding strains and stresses, respectively. The maximal deformations correspond to the deformation achieved at the failure of the test samples. Three test samples per design configuration were tested, and the values given correspond to their arithmetic mean value.

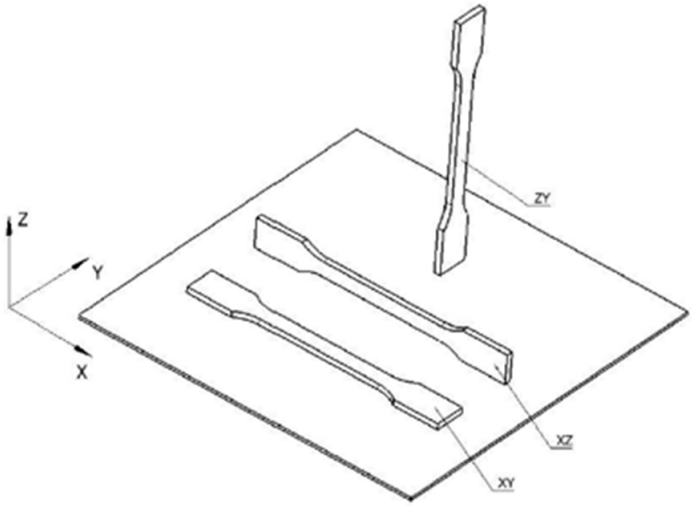

Figure 3. Printing directions for the samples used in tensile tests.

2.5. Density Measurements

The density of the samples printed in *XY*, *YX*, *YZ*, *ZY*, *XZ*, and *ZX* directions were determined at the University of Latvia at room temperature (22 °C) by using hydrostatic weighing in isopropyl alcohol and Mettler Toledo XS205DU balance with a precision of ±0.05 mg. First, the density of isopropyl alcohol was determined by using a sinker of a known volume of 10 cm^3. Then the mass of the samples was registered in the air (m_a) and a liquid of known density (m_l). The density of the samples was determined by the formula:

$$\rho = \frac{m_a}{m_a - m_l}(\rho_l - \rho_a) + \rho_a, \quad (2)$$

where ρ_l and ρ_a are the density of the liquid (0.785 g/cm^3 for isopropyl alcohol) and the air (0.0012 g/cm^3 for air). Three samples per printing direction were weighed in air and isopropyl alcohol, and the values provided in the paper correspond to their arithmetic mean value accomplished by the standard deviation.

2.6. Microscopy Analysis

The morphology of the surface was evaluated for the test samples printed in *XY*, *YZ*, and *XZ* directions using a desktop scanning electron microscope (SEM) Phenom Pro in the Institute of Solid State Physics. Images were taken with a backscattered electron detector (BSD) using an accelerating voltage of 5 kV.

Freely available ImageJ analysis [24] was used to evaluate the size distribution of the 3D-printed "grains" on the fracture surfaces. By using an iso-data algorithm, the optimum brightness threshold was obtained, and the image was divided into filler particles (3D-printed grains) and background (voids) by the comparison of average brightness below and after the set test threshold value [25,26]. Thus, the 3D-printed grains were separated from the background by setting the brightness threshold between them and the background. The area of grains was defined via the number of pixels for each micrograph and was used for the subsequent histogram analysis.

3. Results and Discussion

3.1. Vertical Burn Tests

The results obtained for the vertical burn tests for the samples printed in the *XY*, *XZ*, *ZY*, *XY* ± 45°, and *ZX* ± 45° directions are shown in Figure 4a in relation to sample thickness. As described before, the average burn length shall not exceed 152 mm to pass a 60-s vertical burn test. According to the results provided in Figure 4a, all 3D-printed

samples passed this criterion and could be applied in the interior of aircraft, meeting all requirements for flammability formulated in FAR 25.853 and FAR 25.855 [6,7].

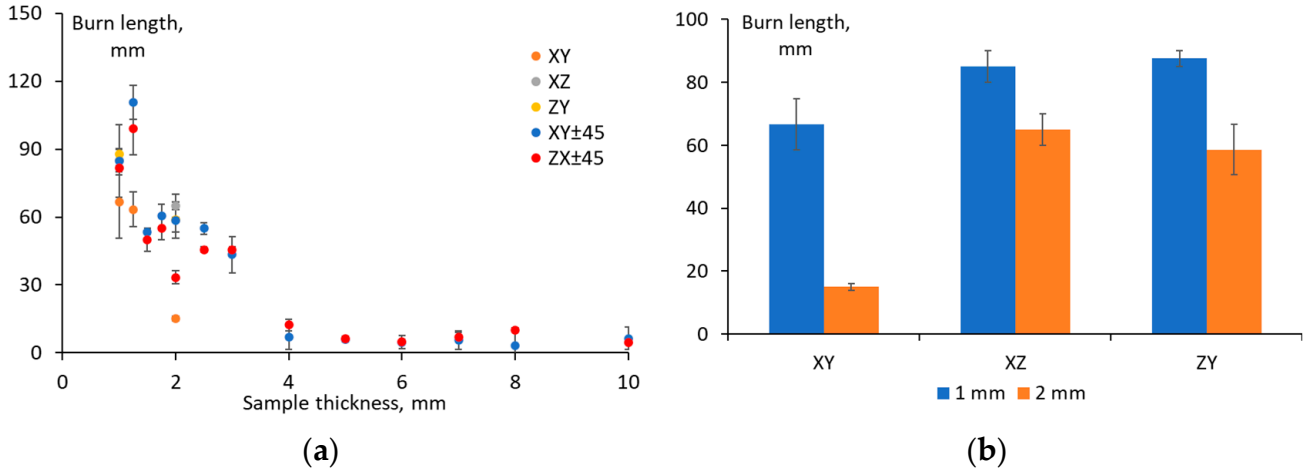

Figure 4. Burn length as a function of sample thickness for different printing directions, as indicated on graph (**a**), and burn length as a function of printing directions, as indicated on the graph for the samples of thickness 1 and 2 mm (**b**).

Moreover, it is obvious from Figure 4 that, with the increase in thickness, the burn length decreases. Similar results have been obtained previously [9,23], and were explained by the fact that the greater the mass of the printed material, the higher the fire resistance and the lower the burn length. After the sample thickness of 4 mm, the burn length was almost constant (~5–7 mm). Therefore, the difference may exist only for thin samples, e.g., of thickness 1 and 2 mm. These results were compared for the samples printed in *XY*, *XZ* and *ZY* directions and are provided in Figure 4b. According to Figure 4b, the effect of printing direction was significant at small thicknesses. The smallest burn length was denoted for *XY* printing direction for both sample thicknesses. For the sample thicknesses of 1 mm and 2 mm, the burn length was reduced by 1.5 and 4 times, accordingly, if the *XY* printing direction is compared with the *XZ* and *ZY* ones. Therefore, despite expected isotropy for the samples produced by SLS technology, *XY* printing direction provides samples demonstrating the best performance for flammability. This could be explained by the reduced content of defects/voids, which was identified by the microscopy analysis.

3.2. Tensile Tests

The representative stress-strain curves for the PA 2241 FR samples printed in different directions are provided in Figure 5a. Similar results were obtained for other samples of the same printing directions. From these curves, it can be observed that the effect of printing direction on the mechanical behaviour was not substantial. The quantitative results obtained for the elastic modulus, tensile strength, and maximal deformation are summarized in Figure 5b. According to Figure 5b, the elastic modulus and tensile strength of the samples printed in *XY* and *YX* directions were slightly higher—by 3% and 2%, respectively, than the same parameters for the samples printed in the other directions.

These results indicate a rather homogeneous structure of the samples when they are printed at a certain thickness (4 mm for the tensile tests). All results obtained for the tensile characteristics of PA 2241 FR conform to the data provided by the supplier [21].

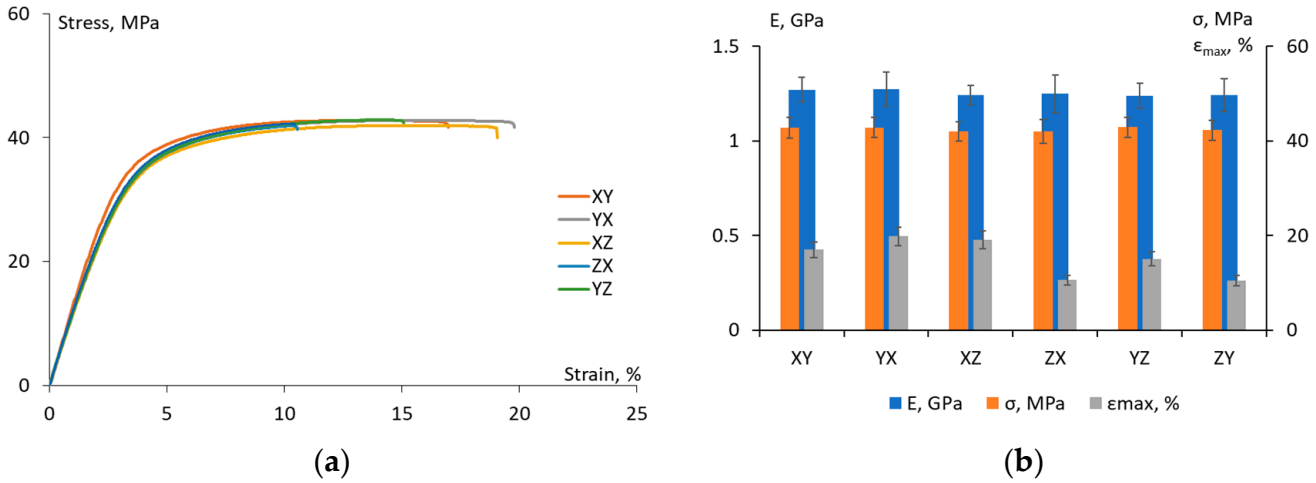

Figure 5. Representative stress-strain curves (**a**) and tensile characteristics (**b**) for the samples printed in different directions, as indicated on the graph.

3.3. Density Evaluation

The experimental results for the density of the samples printed in different directions revealed no significant effect of the printing direction (see Table 2). Again, for the samples printed in the *XY* and *YX* directions, the results were slightly higher, but they could be neglected considering such a negligible effect on the density and standard deviation of 0.01 g/cm^3. According to the data provided by the supplier, the density of PA 2241 FR is 1.00 g/cm^3 [21], which is in line with the results obtained in this work. Thus, it can be concluded that density was also not affected by the printing direction.

Table 2. Density of the samples printed in different directions.

Printing Direction	Density, g/cm^3
XY	1.027 ± 0.007
YX	1.026 ± 0.005
XZ	1.023 ± 0.008
ZX	1.023 ± 0.006
YZ	1.023 ±0.005
ZY	1.023 ±0.007

3.4. Microscopy Analysis

Generally, the properties of 3D-printed polymer composites are dependent not only on the properties of the polymers but also on the material microstructure: the angle of printing and the thickness of the layers, as well as the interactions between the layers [27]. Some morphological peculiarities of the test sample printed in the *XY*, *ZX*, and *YZ* directions can be observed from Figure 6.

Obviously, the fracture surfaces for all samples were rather smooth, indicating a brittle fracture that is typical for polyamides at room temperature, although some roughness and "grainy" structures were also detected for all samples. Their size and distribution were different between the samples, with the most evident dominance for the *XZ* direction. A similar granulated nature for the fracture surfaces was reported at low temperatures for polyamide 12 reinforced with short glass fibres [19], which was attributed to larger thermal contraction of the matrix compared to the fibres, and the granules' size was similar to the original powder (50–100 μm). In general, our results could indicate a reduced quality of printing in the *XZ* direction by using SLS technologies, resulting in a higher content of voids compared to the *XY* and *YZ* printing directions.

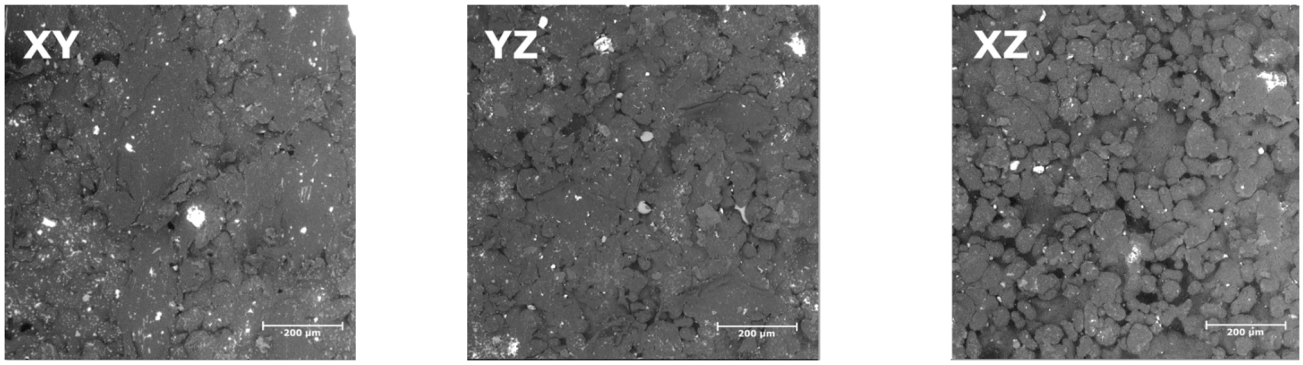

(**a**) (**b**) (**c**)

Figure 6. Typical micrographs of fracture surface for the test samples printed in *XY* (**a**), *YZ* (**b**), and *XZ* (**c**) directions.

To investigate the distribution of 3D-printed "grains" on the fracture surface, the obtained area of all individual grain particles was used for the histogram analysis. The results obtained are provided in Figure 7, revealing a higher number of filler (grain) particles within the range of area from 10 to 90 µm^2 for the samples printed in the *XY* and *YZ* directions in comparison with the *XZ* direction. The lower number of particles in this range indicates a higher content of voids, which is also obvious from Figure 6c. However, it should be noted that the analysis is limited by a small area rejecting the rest of the specimen, and therefore this area should be representative of the whole specimen [25].

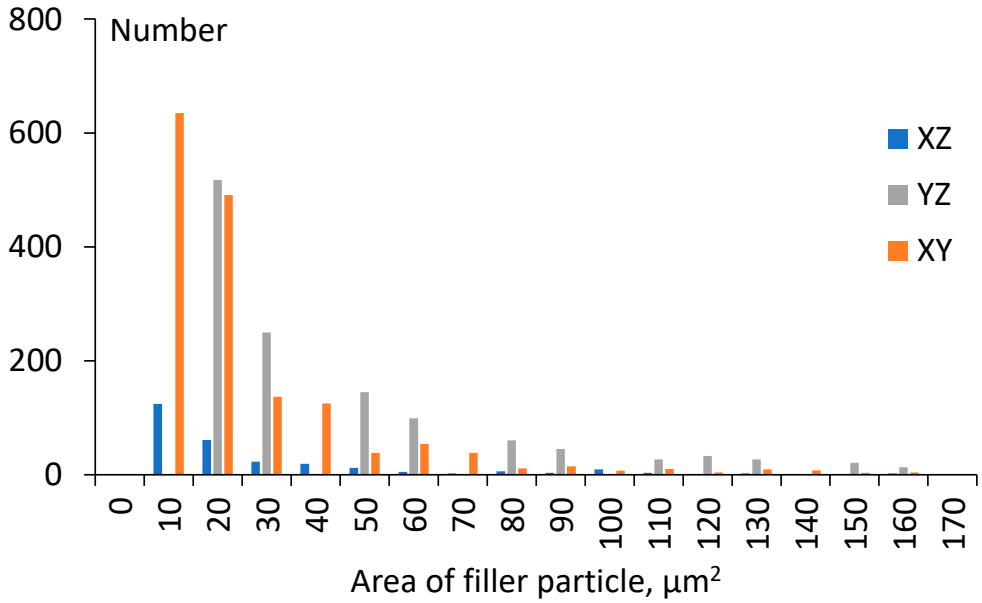

Figure 7. Filler particle's area distribution for the samples printed in different directions (indicated on the graph).

Nevertheless, for all test samples, the results of SEM revealed some inhomogeneities ("grainy" structures and voids) that could lead to anisotropy in the physical properties, especially within the long-term use when environmental factors (e.g., absorbed moisture and temperature) could affect the structure and deteriorate the mechanical properties [27,28].

4. Conclusions

Efforts were made to evaluate the effect of printing direction on the flame-retardant and tensile properties of polyamide 12 processed by selective laser sintering.

It was experimentally confirmed that the burn length of the samples printed at all thicknesses starting from 1 mm and until 10 mm meets the requirements set in FAR standards No. 25.853 and 25.855 for compartment aircraft interiors. It was revealed that the burn length was affected by the printing direction at thicknesses of 1 and 2 mm, while after the sample thickness of 4 mm, the burn length was almost constant for all printing directions. This could be described by the scale factor and anisotropy for the thinner samples produced by SLS technology.

The morphological peculiarities of the test samples printed in different directions were examined by SEM and revealed some inhomogeneities (voids) for all of them. This should be taken into account considering the long-term use of these materials because environmental factors could deteriorate the mechanical properties.

No significant influence of printing direction was established on the tensile and density characteristics, proving homogeneous structure and the same properties at micro-scale for polyamide 12 processed by SLS technology. Moreover, because all samples passed the vertical burn tests, the manufacturing of the interior parts can also have partial infill, thus minimizing the weight of the parts and leading to a total weight reduction and fuel savings for aircraft.

Author Contributions: The study concept was devised by D.D.; methodology, validation, and formal analysis were carried out by D.D., J.J. and T.G.-K.; the investigation, resources, and data curation were performed by D.D., T.G.-K., L.L., S.K., A.S. and A.Z.; writing—original draft preparation was performed by T.G.-K., P.-P.K., A.S. and A.Z.; supervision was performed by D.D.; project administration was performed by D.D. and J.J. All authors have read and agreed to the published version of the manuscript.

Funding: This research was funded by the European Regional Development Fund within Measure 1.1.1.1 "Industry-Driven Research" of the Specific aid objective 1.1.1 "To increase the research and innovation capacity of scientific institutions of Latvia and their ability to attract external funding by investing in human resources and infrastructure" of the Operational Program "Growth and Employment" (Project No. 1.1.1.1/19/A/143). A.S. and A.Z. are grateful to funding received from the European Union Horizon 2020 Framework programme H2020-WIDESPREAD-01-2016-2017-TeamingPhase2 under grant agreement No. 739508, project CAMART2.

Data Availability Statement: The data presented in this study are available on request from the corresponding author.

Conflicts of Interest: The authors declare no conflict of interest.

References

1. Bacciaglia, A.; Ceruti, A.; Liverani, A. Towards large parts manufacturing in additive technologies for aerospace and automotive applications. *Procedia Comput. Sci.* **2022**, *200*, 1113–1124. [CrossRef]
2. Altıparmak, S.C.; Xiao, B. A market assessment of additive manufacturing potential for the aerospace industry. *J. Manuf. Processes* **2021**, *68*, 728–738. [CrossRef]
3. Mohanavel, V.; Ashraff Ali, K.S.; Ranganathan, K.; Allen Jeffrey, J.; Ravikumar, M.M.; Rajkumar, S. The roles and applications of additive manufacturing in the aerospace and automobile sector. *Mater. Today Proc.* **2021**, *47*, 405–409. [CrossRef]
4. Kobenko, S.; Dejus, D.; Jātnieks, J.; Pazars, D.; Glaskova-Kuzmina, T. Structural integrity of the aircraft interior spare parts produced by additive manufacturing. *Polymers* **2022**, *14*, 1538. [CrossRef]
5. Hajare, D.M.; Gajbhiye, T.S. Additive manufacturing (3D printing): Recent progress on advancement of materials and challenges. *Mater. Today Proc.* **2022**, *in press*. [CrossRef]
6. Federal Aviation Regulation (FAR). Standard No. 25.853 Fire Test to Aircraft Material: Fire Protection for Compartment Interior. Available online: https://www.federalregister.gov/documents/2019/07/03/2019-13646/interior-parts-and-components-fire-protection-for-transport-category-airplanes (accessed on 15 April 2022).
7. Federal Aviation Regulation (FAR). Standard No. 25.855 Fire Test to Aircraft Material: Cargo or Baggage Compartments. Available online: https://www.govinfo.gov/content/pkg/CFR-2010-title14-vol1/pdf/CFR-2010-title14-vol1-sec25-855.pdf (accessed on 15 April 2022).
8. Chai, M. Flammability Performance of Bio-Derived Composite Materials for Aircraft Interiors 2014. Ph.D. Thesis, University of Auckland, Auckland, New Zealand. Available online: https://researchspace.auckland.ac.nz/handle/2292/24756?msclkid=903aa79abcb011ecabb550fdeea7dd12 (accessed on 15 April 2022).

9. Lv, Y.; Dejus, D.; Kobenko, S.; Singamneni, S.; Glaskova-Kuzmina, T. Evaluation of the fire-retardancy of ULTEM 9085 polymer composites processed by fused deposition modelling. *Mater. Sci.* 2022, *in press*. [CrossRef]
10. Babrauskas, V.; Peacock, R.D. Heat Release Rate. The Single Most Important Variable in Fire Hazard. *Fire Saf. J.* **1992**, *18*, 255–272. [CrossRef]
11. Price, D.; Anthony, G.; Carty, P. Introduction: Polymer Combustion, Condensed Phase Pyrolysis and Smoke Formation. In *Fire Retardant Materials*; Horrocks, R., Price, D., Eds.; Woodhead Publishing Limited: Cambridge, UK, 2001; pp. 1–30. [CrossRef]
12. Awad, A.; Fina, F.; Goyanes, A.; Gaisford, S.; Basit, A.W. 3D printing: Principles and pharmaceutical applications of selective laser sintering. *Int. J. Pharm.* **2020**, *586*, 119594. [CrossRef]
13. Ma, F.; Zhang, H.; Hon, K.K.B.; Gong, Q. An optimization approach of selective laser sintering considering energy consumption and material cost. *J. Clean. Prod.* **2018**, *199*, 529–537. [CrossRef]
14. Batistella, M.; Regazzi, A.; Pucci, M.F.; Lopez-Cuesta, J.-M.; Kadri, O.; Bordeaux, D.; Ayme, F. Selective laser sintering of polyamide 12/flame retardant compositions. *Polym. Degrad. Stab.* **2020**, *181*, 109318. [CrossRef]
15. Schneider, K.; Wudy, K.; Drummer, D. Flame-retardant polyamide powder for laser sintering: Powder characterization, processing behavior and component properties. *Polymers* **2020**, *12*, 1697. [CrossRef]
16. Durgun, I.; Ertan, R. Experimental investigation of FDM process for improvement of mechanical properties and production cost. *Rapid Prototyp. J.* **2014**, *20*, 228–235. [CrossRef]
17. Wu, W.; Geng, P.; Li, G.; Zhao, D.; Zhang, H.; Zhao, J. Influence of layer thickness and raster angle on the mechanical properties of 3D-printed PEEK and a comparative mechanical study between PEEK and ABS. *Materials* **2015**, *8*, 5834–5846. [CrossRef] [PubMed]
18. Sood, A.K.; Ohdar, R.K.; Mahapatra, S.S. Parametric appraisal of mechanical property of fused deposition modeling processed parts. *Mater. Des.* **2010**, *31*, 287–295. [CrossRef]
19. Salazar, A.; Rico, A.; Rodríguez, J.; Segurado Escudero, J.; Seltzer, R.; Martin de la Escalera Cutillas, F. Fatigue crack growth of SLS polyamide 12: Effect of reinforcement and temperature. *Compos. Part B* **2014**, *59*, 285–292. [CrossRef]
20. Salmoria, G.V.; Paggi, R.A.; Lago, A.; Beal, V.E. Microstructural and mechanical characterization of PA12/MWCNTs nanocomposite manufactured by selective laser sintering. *Polym. Test.* **2011**, *30*, 611–615. [CrossRef]
21. Technical Data Sheet for PA 2241 FR. EOS. Available online: https://www.eos.info/en/additive-manufacturing/3d-printing-plastic/sls-polymer-materials/polyamide-pa-12-alumide (accessed on 15 April 2022).
22. Technical Data Sheet for EOS P 396 SLS Machine. EOS. Available online: https://www.eos.info/en/additive-manufacturing/3d-printing-plastic/eos-polymer-systems/eos-p-396 (accessed on 15 April 2022).
23. *ISO 527-1*; Plastics—Determination of Tensile Properties—Part 1: General Principles. ISO: London, UK, 2019. Available online: https://www.iso.org/standard/75824.html (accessed on 3 May 2022).
24. Rasband, W. ImageJ-National Institute of Health, USA. 1997. Available online: http://rsb.info.nih.gov/ij/ (accessed on 25 May 2022).
25. Glaskova, T.; Zarrelli, M.; Borisova, A.; Timchenko, K.; Aniskevich, A.; Giordano, M. Method of quantitative analysis of filler dispersion degree in composite systems with spherical inclusions. *Compos. Sci. Technol.* **2011**, *71*, 1543–1549. [CrossRef]
26. Glaskova, T.; Zarrelli, M.; Aniskevich, A.; Giordano, M.; Trinkler, L.; Berzina, B. Quantitative optical analysis of filler dispersion degree in MWCNT-epoxy nanocomposite. *Compos. Sci. Technol.* **2012**, *72*, 477–481. [CrossRef]
27. Ngoa, T.D.; Kashania, A.; Imbalzanoa, G.; Nguyena, K.T.Q.; Hui, D. Additive manufacturing (3D printing): A review of materials, methods, applications and challenges. *Compos. Part B* **2018**, *143*, 172–196. [CrossRef]
28. Glaskova, T.; Aniskevich, A. Moisture effect on deformability of epoxy/montmorillonite nanocomposite. *J. Appl. Polym. Sci.* **2010**, *116*, 493–498. [CrossRef]